JACS
JOURNAL OF THE AMERICAN CHEMICAL SOCIETY
Article
Cite This: J. Am. Chem. Soc. 2019, 141, 3232−3239
pubs.acs.org/JACS

Unifying the Hydrogen Evolution and Oxidation Reactions Kinetics in Base by Identifying the Catalytic Roles of Hydroxyl-Water-Cation Adducts

Ershuai Liu,[†] Jingkun Li,[†] Li Jiao,[‡] Huong Thi Thanh Doan,[†] Zeyan Liu,[§] Zipeng Zhao,[§] Yu Huang,[§,∥] K. M. Abraham,[†] Sanjeev Mukerjee,[†] and Qingying Jia*[,†]

[†]Department of Chemistry and Chemical Biology, Northeastern University, Boston, Massachusetts 02115, United States
[‡]Department of Chemical Engineering, Northeastern University, Boston, Massachusetts 02115, United States
[§]Department of Materials Science and Engineering, University of California, Los Angeles, California 90095, United States
[∥]California NanoSystems Institute (CNSI), University of California, Los Angeles, California 90095, United States

Supporting Information

ABSTRACT: Despite the fundamental and practical significance of the hydrogen evolution and oxidation reactions (HER/HOR), their kinetics in base remain unclear. Herein, we show that the alkaline HER/HOR kinetics can be unified by the catalytic roles of the adsorbed hydroxyl (OH_{ad})-water-alkali metal cation (AM^+) adducts, on the basis of the observations that enriching the OH_{ad} abundance via surface Ni benefits the HER/HOR; increasing the AM^+ concentration only promotes the HER, while varying the identity of AM^+ affects both HER/HOR. The presence of OH_{ad}-$(H_2O)_x$-AM^+ in the double-layer region facilitates the OH_{ad} removal into the bulk, forming OH^--$(H_2O)_x$-AM^+ as per the hard−soft acid−base theory, thereby selectively promoting the HER. It can be detrimental to the HOR as per the bifunctional mechanism, as the AM^+ destabilizes the OH_{ad}, which is further supported by the CO oxidation results. This new notion may be important for alkaline electrochemistry.

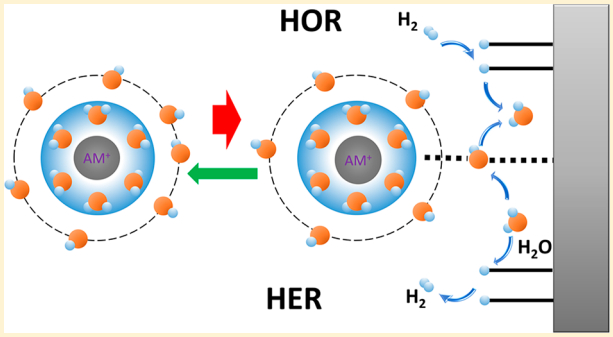

INTRODUCTION

The hydrogen evolution and oxidation reactions (HER/HOR) hold the key to the future hydrogen economy by controlling efficient generation of hydrogen from water and the reverse direction to harvest clean energy. They are also the most fundamental electrochemical reactions wherein the Butler−Volmer equation[1] and the Sabatier's principle[2] were initially verified in low-pH media. Despite their significance in both practical and fundamental aspects, the HER/HOR kinetics in base has been elusive and clouded by several long-standing puzzles. It is unclear why the HER/HOR rates of some transition metals including Pt, Ir, and Pd in base are 2 orders of magnitude slower than in acid[3] and why they are sensitive to the surface structure.[4] While it is certain that mixing Pt with some metals such as Ru or Ni can improve the HER and/or HOR rates,[5−11] it is uncertain why. These puzzles also inhibit the rational design of electrocatalysts for the alkaline HER/HOR.

Currently there are three schools of thought on the HER/HOR kinetics in base. The central argument of each thought and the key discrepancies within them can be well illustrated by the Pt−Ni systems. The hydrogen binding energy (HBE) theory states that the binding energy between the metal and the hydrogen ($E_{M\text{-}H}$) dictates the inherent HER/HOR activity of the metal. Accordingly, the superior HOR activity of the PtNi/C alloy nanoparticles (NPs) to that of Pt/C NPs was ascribed to the optimization of the E_{Pt-H} by the Ni underneath rather than on the Pt surface.[7] A similar argument was also proposed on the Pt−Ru system.[6,10] A key aspect of the HBE theory is that the second metal does not need to be on the surface to promote the HER/HOR.[6,10] However, unambiguous *in situ* evidence for Pt-bimetallic systems with clean Pt surfaces free of the second metal during the HER/HOR is missing.[11] The HBE theory was also adopted to account for the pH-dependent and structure-dependent HER/HOR rates. It was found that the HER/HOR rates of the Pt(100) and Pt(110) within a pH range of 0−13 were linearly related to the position of the underpotential-deposited hydrogen (H_{UPD}) desorption peak (E_{peak}) that was believed to be linearly related to $E_{M\text{-}H}$.[12] However, emerging evidence shows that the E_{peak} is not solely determined by the $E_{M\text{-}H}$ but also by the metal−OH_{ad} bond strength (E_{M-OH}) for stepped Pt surfaces.[13,14] As for the Pt(111) surface free of OH_{ad} within the H_{UPD} potential region, the E_{peak} is pH-independent (e.g., regular Nernstian shift with pH), whereas the HER/HOR activity still shifts with pH like

Received: December 11, 2018
Published: January 23, 2019

DOI: 10.1021/jacs.8b13228
J. Am. Chem. Soc. 2019, 141, 3232−3239

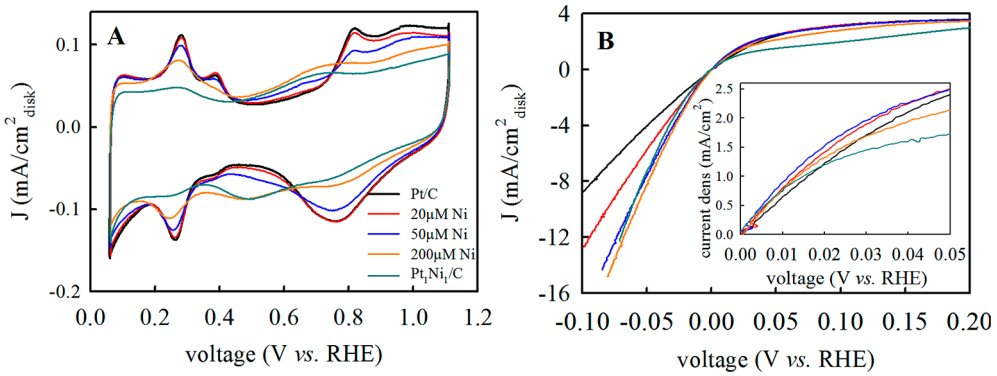

Figure 1. CV (A) and IR-corrected HER/HOR polarization curves (B) collected at room temperature in an Ar/H_2-saturated 0.1 M KOH electrolyte on the Pt/C with varied concentrations of Ni^{2+} and the Pt_1Ni_1/C alloy. The inset in B displays the zoomed-in HOR kinetic region. Cathodic scans were chosen for all the HER/HOR curves presented owing to their superior rates to anodic scans.

stepped Pt surfaces.[15] Koper et al.[15,16] noticed that the E_{peak} shifts with pH the same way as the potential of zero free charge (pzfc) for both extended and stepped Pt surfaces and proposed that the pH-dependent pzfc likely accounts for the pH-dependent HER/HOR rates of all Pt surfaces (denoted as pzfc theory). As the pzfc shifts positively with increasing pH, the HER/HOR potential is more negative to the pzfc, leading to larger reorganization energy of interfacial water to shuffle OH^- throughout the double layer. Resultantly, the energetic barrier of the Volmer step ($H_2O + e^- \leftrightarrow H_{ads} + OH^-$) for Pt surfaces increases with pH. Accordingly, Koper et al.[15] attributed the improved HER rate of Pt(111) via surface deposition of Ni to the negative shift of the pzfc that was verified by the laser-induced temperature-jump experiment. The pzfc theory is in line with the Frumkin effect,[17] wherein the adsorption of cations positively shifts the potential of the outer Helmholtz plane, thereby promoting the reactions involving transport of anions, such as the Volmer step in base. Alternatively, Markovic et al.[8,18,19] ascribed the Ni-induced enhancement of the HER/HOR rate of Pt(111) to the bifunctional mechanism wherein the surface Ni species promotes H_2O dissociation for the HER and the H_{ad} oxidation for the HOR by hosting OH_{ad}. Unlike the HBE theory, both the bifunctional mechanism and the pzfc theory require the second metal to be present on the surface to promote the alkaline HER/HOR. The key difference between these two notions is that the Ni species directly participates in the HER/HOR for the bifunctional mechanism but not for the pzfc theory. Apparently, a clear understanding of the alkaline HER/HOR kinetics relies on definitive characterization of the second metal *in situ* during the HER/HOR and clear-cut identification of its catalytic roles.

RESULTS AND DISCUSSION

Given that the three aforementioned views have been proposed based on the Pt−Ni system, herein we also chose this system to elucidate the governing mechanism of the alkaline HER/HOR, with strategies allowing for surface deposition of Ni onto Pt surfaces and *in situ* characterization of the surface Ni during the HER/HOR. The HER/HOR of Pt/C NPs (Tanaka Kikinzoku Kogyo, 47.2 wt %) in 0.1 M KOH was assessed in a rotating disk electrode (RDE) as a baseline. The RDE electrode was then immersed into the $Ni(ClO_4)_2$ solution for surface Ni deposition prior to the RDE testing. By repeating this process with gradually increased $Ni(ClO_4)_2$ concentration from 20 to 200 μM, the cyclic voltammetry (CV) features of Pt/C gradually approach those of the Pt_1Ni_1/C alloy (E-Tek, 30 wt %). Specifically, the broad peaks around 0.5−0.6 V_{RHE} arising from the desorption/adsorption of OH^- on surface Ni species emerge,[8] and the intensity of the Pt H_{UPD} peaks decreases (Figure 1A). These results verify that the surface coverage of Ni can be gradually increased in a controlled manner via this approach.

Clear enhancement of the HER/HOR rates of Pt/C was observed when immersed in 20 μM $Ni(ClO_4)_2$ (Figure 1B), whereas the CV remains largely unperturbed due to the slight adsorption of Ni. The Ni-induced HER/HOR promotion against the minimal disturbance of the Pt surface bypasses the dilemma of proper evaluation of the electrochemical surface area for the HER/HOR in base,[20] thus conclusively showing that surface Ni improves the HER/HOR kinetics of Pt/C. These results agree with previous observations that surface deposition of $Ni(OH)_2$ improves the HER/HOR rate of Pt(111).[8,9] In addition to the promoting effect, the surface Ni also has a detrimental effect on the HER/HOR of Pt/C by blocking the Pt surface, which is evidenced by the reduced intensity of the Pt H_{UPD} peaks (Figure 1A) and the HOR limiting currents (Figure 1B, inset) with increasing Ni content. As a result of the counterbalance of the two opposite effects, the HER improvement slows down with increasing Ni coverage, and the HOR rate exhibits a volcano trend (Figure 1B). Both the HER/HOR rates approach those of the Pt_1Ni_1/C with increasing Ni coverage, which strongly suggests that the HER/HOR of the Pt_1Ni_1/C alloy is dictated by the surface Ni rather than the Ni underneath. This remark contradicts the previous claim that it was not the surface Ni but the subsurface Ni of the PtNi/C alloy that promotes the HOR.[7] We found that the acid immersion treatment applied there was insufficiently harsh to remove all the surface Ni species from the Pt_1Ni_1/C NPs (Figure S1). If a typical CV activation process was used to eliminate surface Ni species,[21] the HER/HOR rate was significantly reduced and slower than that of Pt/C, whereas the oxygen reduction reaction (ORR) rates in both acid and alkaline media were much higher (Figure S2). These results suggest that the Ni underneath significantly improves the ORR via strain effects, as supported by *in situ* X-ray absorption spectroscopy (XAS) (Figures S3 and S4 and Table S1), but not the HER/HOR.

The deposition approach is also suitable for physicochemical characterizations since the deposited Ni is exclusively located on the surface and fully exposed to the electrochemical environment. The all-surface configuration free of the "bulk"

DOI: 10.1021/jacs.8b13228
J. Am. Chem. Soc. 2019, 141, 3232−3239

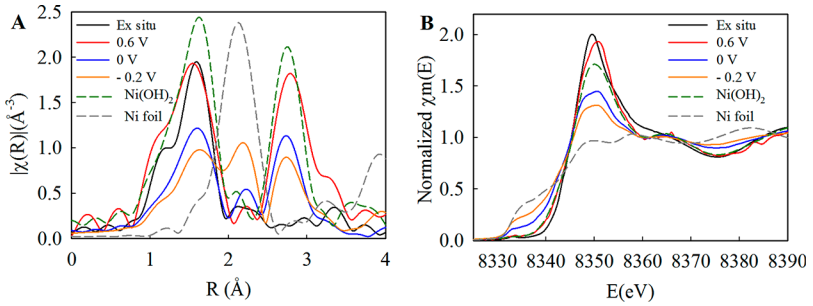

Figure 2. FT-EXAFS (A) and XANES (B) spectra at the Ni K-edge of the $Ni(ClO_4)_2$ deposited onto Pt/C as a function of applied potentials collected in a H_2-purged 0.1 M KOH electrolyte, together with those of Ni^0 foil and $Ni(OH)_2$ as references.

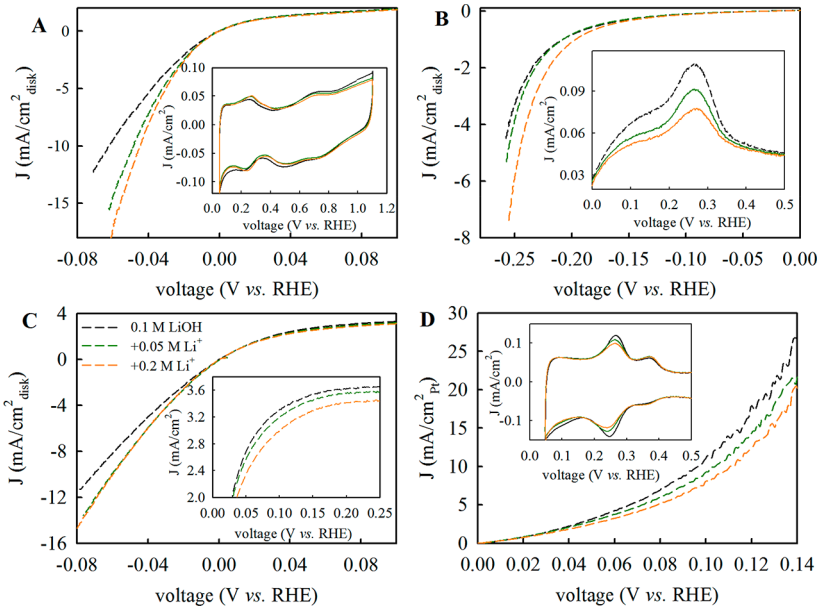

Figure 3. HER/HOR polarization curves of (A) Pt_1Ni_1/C, (B) Ni/C, and (C) Pt/C collected in H_2-saturated 0.1 M LiOH with varying concentration of $LiClO_4$. (D) HOR kinetic currents normalized by the H_{UPD} area of Pt/C. The insets in A, B, and D present the CV curves of Pt_1Ni_1/C, Ni/C, and Pt/C, respectively, and that in C presents the limiting currents of the HOR of Pt/C. Note the scale of the *y* axis in D is linear rather than log to highlight the difference. The regular Tafel plot with log scale is given in Figure S10.

Ni allows for surface characterization of the Ni by a bulk technique such as XAS. In parallel to the RDE tests, the Pt/C electrode was subject to XAS measurements before and after immersing into the $Ni(ClO_4)_2$ solution in 0.1 M H_2-saturated KOH as a function of applied potentials. The *ex situ* Fourier transform of the extended X-ray absorption fine structure (FT-EXAFS) spectrum of the Ni deposited onto Pt/C at the Ni K-edge shows only one prominent peak around 1.5 Å overlapping the Ni−O peak of $Ni(OH)_2$ (Figure 2A). The lack of Ni−Ni or any other long-range order scattering peaks indicates the predominant presence of the isolated single atom moiety of $Ni-O_6$, which is further confirmed by the EXAFS fitting with a Ni−O coordination number of 5.7 ± 0.7 and bond distance of 2.05 ± 0.01 Å (Figure S5 and Table S2). Correspondingly, the intensity of the Ni X-ray absorption near-edge structure (XANES) spectrum of the deposited Ni is higher than that of the $Ni(OH)_2$ standard (Figure 2B), indicating a high oxidation state, as expected from the $Ni-O_6$ configuration. On the other hand, the *ex situ* XAS of the Ni/C NPs shows coexistence of reduced Ni^0 and Ni^{2+} oxide species as expected from the particle configuration that the exposed Ni is in the form of oxides, whereas the Ni underneath is in the reduced form of Ni^0 (Figure S3). The unitary configuration of $Ni-O_6$ of the deposited Ni indicates the nearly full exposure of the Ni atoms to the air.

Further *in situ* XAS measurements show that the deposited Ni changes from $Ni-O_6$ to a mixture of reduced Ni^0 and Ni^{2+} oxides with applied potentials, and the two species exchange with each other with changing potentials. At 0.6 V_{RHE}, a prominent peak emerges around 2.7 Å overlapping the Ni−Ni peak of $Ni(OH)_2$ (Figure 2A), indicating the formation of Ni^{2+} oxides. As the potential shifts negatively to −0.2 V_{RHE}, the intensity of the Ni−O (1.5 Å) and Ni−Ni (2.7 Å) peaks associated with $Ni(OH)_2$ decreases, whereas the Ni−Ni peak (2.2 Å) from the Ni^0 metal emerges (Figure 2A). Concurrently, the intensity of the XANES spectra gradually decreases, approaching that of the Ni foil (Figure 2B). These reversible trends are also observed on the Ni/C NPs, except that the Ni^0 signals are present throughout the whole potential region owing to the presence of Ni^0 metal in the core (Figure S6). *In situ* XAS thus provides conclusive evidence that the surface Ni in both cases is in the mixed form of Ni^{2+} oxides and reduced Ni^0 and undergoes the Ni^{2+}/Ni^0 redox transition associated with adsorption/desorption of oxygen species during the HER/HOR. This finding disagrees with Markovic et al.'s previous finding[8,9] that the surface-deposited Ni remains

DOI: 10.1021/jacs.8b13228
J. Am. Chem. Soc. 2019, 141, 3232−3239

mostly in the form of redox-inactive Ni^{2+} without forming Ni^0 at negative potentials. It is noted that their conclusion was derived from the XANES spectra, whereas ours was based on the combined XANES and FT-EXAFS spectra wherein the FT-EXAFS clearly shows the transition between Ni^{2+} and Ni^0 with changing potentials (Figure 2a). The generation of Ni^0 at negative potentials accounts for the lower intensity of the XANES spectra compared to that of the $Ni(OH)_2$ standard seen here and previously.[9]

The rich redox behavior of the surface Ni during the HER/HOR indicates that the Ni can exchange oxygen species (OH_{ad}) with the electrolyte at HER/HOR relevant potentials and may thus promote the HER/HOR kinetics.[8,18,22] Given the possible interactions between the OH_{ad} and the hydrated alkali metal cations (AM^+),[23,24] we added $LiClO_4$ into the 0.1 M LiOH electrolyte (K^+ was not chosen because of the low solubility of $KClO_4$) to gradually increase the Li^+ concentration, followed by the HER/HOR measurements to probe the roles of OH_{ad}. Since the electrolyte resistance decreases with increasing Li^+ concentration (Figure S7), all the HER/HOR curves displayed are IR-corrected for the kinetics study. For both the Pt_1Ni_1/C alloy (Figure 3A) and the Pt/C with deposited Ni (Figure S8), the HER rates increase markedly with increasing Li^+ concentration, in line with the previous observation that adding Li^+ improves the HER of the Pt(111) with surface-deposited $Ni(OH)_2$ ($Ni(OH)_2$/Pt(111)).[9] On the other hand, the HOR rate remains unaffected (Figure 3A). The same trends were observed with increasing Na^+ concentration (Figure S9).

To decipher the Li^+-induced selective enhancement of the HER of Pt_1Ni_1/C, the same experiment was conducted on Ni/C and Pt/C, separately. With increasing Li^+ concentration, the HER rate of Ni/C increases markedly, and the intensity of the Ni redox peak around 0.27 V_{RHE} decreases (Figure 3B, inset). Similarly, the HER rate of Pt/C also increases with Li^+ concentration, and the intensity of the H_{UPD} peaks decreases (Figure 3D, inset). The concurrent decrease of the HOR limiting current, despite the increase of the viscosity of the electrolyte with increasing Li^+ concentration, indicates that the Li^+-induced blocking effect makes less Pt sites participate in the HOR. These results suggest that the Li^+ ions are stabilized onto the surface blocking active sites, and the stabilized Li^+ facilitates the HER. This argument is further strengthened by the finding that the Li^+ has no effect on the HER/HOR of the Pt(111) surface that does not bind Li^+ within the HER/HOR kinetic potential region.[24] Unlike Pt/C, neither the Pt H_{UPD} peak intensity nor the HOR limiting current intensity of the Pt_1Ni_1/C decreases with increasing Li^+ concentration (Figure 3A and inset), whereas the intensity of the peaks associated with the desorption/adsorption of OH^- on the Ni surface slightly decreases (Figure 3A, inset). These results suggest that the Li^+ preferentially binds to the surface Ni sites and promotes the HER of Pt_1Ni_1/C. These results are in line with the previous finding that the Li^+ does not affect the HER of Pt(111), but dramatically improves the HER of $Ni(OH)_2$/Pt(111).[9] We thus conclude that the Li^+ promotes the HER of Pt−Ni systems via interacting with Ni.

The selective suppression of the H_{UPD} peak associated with the Pt(110) facet (~0.28 V_{RHE}) (Figure 3D, inset) with increasing Li^+ concentration indicates the stabilization of Li^+ selectively onto stepped facets. These observations can be explained by either the selective adsorption of AM^+ onto stepped Pt surfaces[13,14] or OH_{ad} anchoring hydrated AM^+, forming OH_{ad}-$(H_2O)_x$-AM^+ adducts,[22−24] given that this sharp H_{UPD} peak involves the exchanges of H_{ad} and OH_{ad}.[13,14] *In situ* XAS favors the latter case since the interaction between the AM^+ and Pt or Ni was not observed, whereas abundant oxygen species were present on the surface Ni within the HER/HOR potential region (Figure 2A). Moreover, the AM^+ does not affect the HER/HOR of the Pt(111) free of OH_{ad} at low potentials, but affects the HOR and ORR of Pt(111) at elevated potentials when the surface is covered by OH_{ad},[25] or affects the HER/HOR of $Ni(OH)_2$/Pt(111).[8,9] These phenomena underscore the indispensible role of OH_{ad} rather than stepped Pt surfaces in triggering the catalytic roles of AM^+, thus favoring the notion of the formation of OH_{ad}-$(H_2O)_x$-AM^+ adducts within the double-layer region. Therefore, we endorse the presence of the OH_{ad}-$(H_2O)_x$-AM^+ adduct on surface sites such as Pt(110) or Ni oxides that can host OH_{ad} within the HER/HOR potential region to anchor the hydrated AM^+. Next by identifying the catalytic roles of OH_{ad}-$(H_2O)_x$-AM^+, we unify the alkaline HER/HOR kinetics.

Current interpretations on the catalytic roles of OH_{ad}-$(H_2O)_x$-AM^+ in various electrochemical reactions are incoherent. The OH_{ad}-$(H_2O)_x$-AM^+ adducts were believed to be detrimental to the HOR and ORR at elevated potentials, blocking active sites as spectators.[23−25] Their catalytic and blocking effects are negligible for the HOR within the kinetic potential region (<0.2 V_{RHE}), as shown here on Pt−Ni systems and previously on Ru/C and Ir/C.[23] This phenomenon was explained in terms of the HOR being limited by the metal−H_{ad} binding[23] that is unaffected by AM^+ owing to the lack of interactions between H_{ad} and AM^+,[24] plus a low concentration of OH_{ad} at low potentials.[23] This explanation implicates the negligible roles of OH_{ad}-$(H_2O)_x$-AM^+ in the HER improvement that occurs at even lower potential with presumably even lower concentrations of OH_{ad}. Indeed, the Li^+-induced HER improvement of $Ni(OH)_2$/Pt(111) was not fully ascribed to the presence of OH_{ad}-$(H_2O)_x$-Li^+, but to the promotion of water dissociation.[9] However, not only how the Li^+ promotes water dissociation remains unknown, but this argument is also not favored by recent experimental and computational findings that the presence of AM^+ weakens the Pt−O bond.[13,14]

A complete catalytic cycle of water dissociation involves water molecule cleavage and subsequent removal of the hydroxyl intermediate. Li^+ improves the HER of Pt/C while weakening the Pt−O bond and of Ni/C that binds O overly strong.[26] These results suggest that Li^+ facilitates the OH_{ad} removal rather than water molecule cleavage. By incorporating the concept of OH_{ad}-$(H_2O)_x$-AM^+, these two steps can be written as

$$H_2O + (H_2O)_x\text{-}AM^+ \leftrightarrow H_{ad} + OH_{ad}\text{-}(H_2O)_x\text{-}AM^+ \quad (1)$$

$$OH_{ad}\text{-}(H_2O)_x\text{-}AM^+ + e^- \leftrightarrow OH^-\text{-}(H_2O)_x\text{-}AM^+ \quad (2)$$

The sum of these reactions essentially forms the Volmer step: $H_2O + e^- \leftrightarrow H_{ad} + OH^-$. According to the hard−soft acid−base (HSAB) theory,[27] the AM^+ is a Lewis hard acid and binds strongly with the OH^- that is a Lewis hard base, but binds weakly with the nearly neutral OH_{ad} that is a Lewis soft base. The unbalanced binding energy originating from the unbalanced charge between OH^- and OH_{ad} drives the OH_{ad} desorption into the bulk (eq 2), thereby boosting the Volmer step, but only in one direction. As a result, the presence of

DOI: 10.1021/jacs.8b13228
J. Am. Chem. Soc. 2019, 141, 3232−3239

OH_{ad}-$(H_2O)_x$-AM^+ improves the HER but not the HOR, matching the selective HER enhancement of Pt/C and Pt_1Ni_1/C with increasing Li^+ concentration. On the contrary, the HBE and pzfc theories affect the Volmer step in both directions; thus they cannot account for the AM^+-induced selective improvement of the HER.

The new notion that the presence of OH_{ad}-$(H_2O)_x$-AM^+ promotes the alkaline HER as per the HSAB theory is further testified by tuning the interaction energy within the adducts via varying the identity of the AM^+. The HER rate of a Pt polycrystalline electrode (it was chosen here rather than Pt/C despite the lower concentration of OH_{ad} to avoid experimental uncertainties arising from the catalyst loading variation) decreases in the order LiOH > NaOH > KOH (Figure 4A).

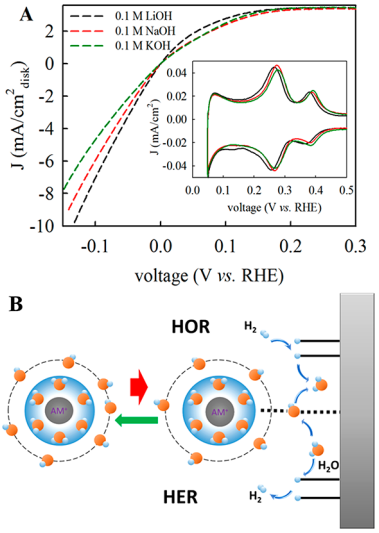

Figure 4. (A) HER/HOR polarization curves of the Pt polycrystalline electrode in H_2-saturated 0.1 M LiOH, NaOH, and KOH. The inset in A presents the CV curves. (B) Schematic illustration of the catalytic roles of OH_{ad}-$(H_2O)_x$-AM^+ in the alkaline HER/HOR kinetics.

According to the HSAB theory, as the Lewis acid hardness decreases in the sequence $Li^+ > Na^+ > K^+$, the interaction energy between OH_{ad} and $(H_2O)_xAM^+$ within OH_{ad}-$(H_2O)_x$-AM^+ increases, whereas the interaction energy between OH^- and $(H_2O)_xAM^+$ within OH^--$(H_2O)_x$-AM^+ decreases. As a result, the interaction energy gap between OH^--$(H_2O)_x$-AM^+ and OH_{ad}-$(H_2O)_x$-AM^+ narrows as $Li^+ > Na^+ > K^+$. Thus, the driving force for the OH_{ad} desorption weakens in the order $Li^+ > Na^+ > K^+$, matching the HER trend of LiOH > NaOH > KOH.

Since the presence of OH_{ad}-$(H_2O)_x$-AM^+ promotes the HER in base, the HER can be improved by enriching the abundance of OH_{ad}-$(H_2O)_x$-AM^+ via increasing the concentration of the OH_{ad} host and/or AM^+. The former case accounts for the enhanced HER with increased surface Ni oxide content (Figure 1B) or with enriched metal−oxide interfaces as widely reported.[28,29] The latter case accounts for the improved HER with increased AM^+ concentration (Figure 3); and the extent of the improvement increasing with the OH_{ad} host abundance: absent for the Pt(111) surface free of OH_{ad},[9] ~20% for Pt/C with some OH_{ad} (−0.05 V_{RHE} with 0.1 M $LiClO_4$) and ~75% for Pt_1Ni_1/C with Ni-induced enrichment of OH_{ad} (Figure 3). Moreover, the fact that the Li^+ improves the HER of $Ni(OH)_2$/Pt(111) but not Pt(111)[9] exclusively supports the bifunctional mechanism wherein the OH_{ad} desorbs from $Ni(OH)_2$ and the H_{ad} forms H_2 on adjacent Pt(111) sites after water dissociation. Therefore, the AM^+-induced and transition metal (TM)-induced HER improvements are unified into the promotional roles of OH_{ad}-$(H_2O)_x$-AM^+ in the Volmer step wherein the TM effectively dissociates the water, easing the generation of H_{ad}, and more importantly the byproduct OH_{ad} anchored by TM is effectively removed with the presence of solvated AM^+.

It is noted that the bifunctional mechanism proposed here in combination with the HSAB theory (namely, 2B theory) differs from that proposed by Markovic et al.[8] previously. They stated that the water dissociation (eq 1) is the rate-determining step (rds), and the role of Ni is facilitating this step. We proposed here that the transportation of OH_{ad} (eq 2) is the rds, and accordingly the primary role of Ni is to anchor and remove OH_{ad} into the bulk electrolyte as per the HSAB theory. The bifunctional mechanism wherein the water dissociation is the rds was recently ruled out by Tang's group based on a rigorous kinetics study.[30,31] However, the 2B theory is not, since the transportation of OH_{ad} is not solely determined by the OH_{ad} binding energy as assumed[30] based on the step $OH_{ad} + e^- \leftrightarrow OH^-$, but also affected by the AM^+ as per the HSAB theory by incorporating the concept of OH_{ad}-$(H_2O)_x$-AM^+. In addition, the concept of OH_{ad}-$(H_2O)_x$-AM^+ also implicates that the AM^+ weakens the Pt−OH_{ad} bond by disrupting the hydrogen bonding between OH_{ad} and H_2O as originally proposed by Janik's[14] and Koper's[13] groups. The weaker bond within OH_{ad}-$(H_2O)_x$-Li^+ signifies weaker disruption, thus accounting for stronger Pt−OH_{ad} binding in LiOH. The dual roles of the AM^+ provide a plausible explanation of the paradox that the exchange of H_{ad} and OH_{ad} is more irreversible for Pt(110) in LiOH than in KOH despite the stronger OH_{ad} binding.[30] Recall that the interaction energy within OH^--$(H_2O)_x$-Li^+ is stronger than in OH^--$(H_2O)_x$-K^+, but weaker in OH_{ad}-$(H_2O)_x$-Li^+ than in OH_{ad}-$(H_2O)_x$-K^+. The larger energy gap facilitates the desorption of OH_{ad}, but not reversely the adsorption of OH_{ad}, and is likely responsible for the higher irreversibility in LiOH than in KOH. When in acid free of adsorbed AM^+, the Pt−OH_{ad} bond is even stronger and the exchange of H_{ad} and OH_{ad} becomes reversible.[30]

Varying the concentration or identity of AM^+ alters the rate of not only the HER but also the HOR. The HOR of Pt/C decreases with increasing Li^+ concentration (Figure 3, inset). While the Li^+-induced blocking effect contributes to the decrease, as evidenced by the reduced limiting current density (Figure 3C, inset), the HOR kinetic current density normalized by the H_{UPD} area still decreases with increasing Li^+ concentration (Figure 3D), suggesting that the Li^+ reduces the inherent HOR activity of Pt/C. Meanwhile, the Pt/C shows better HOR in LiOH than in KOH and NaOH (Figure 4A). Both cases can be accounted for by the presence of OH_{ads}-$(H_2O)_x$-AM^+ in association with the bifunctional mechanism. The bifunctional mechanism was originally adopted by Markovic et al. to account for the improved HOR activity of $Ni(OH)_2$/Pt(111),[18] wherein the OH_{ad} furnished by $Ni(OH)_2$ helps to remove H_{ad} (reverse direction of eq 1), but without experimental evidence for the promoting roles of OH_{ads}. The concept of OH_{ads}-$(H_2O)_x$-AM^+ implicates the possibility to probe the catalytic roles of OH_{ads} using AM^+ as a prober via perturbing the OH_{ads} binding energy. The AM^+-induced destabilization of OH_{ad} proposed by Janik's[14] and Koper's[13] group is strongly supported by the observations that

DOI: 10.1021/jacs.8b13228
J. Am. Chem. Soc. 2019, 141, 3232−3239

the H_{UPD} peak of stepped Pt surfaces shifts to higher potential as a result of weakening the Pt−OH_{ad} bond via (1) increasing pH that promotes the adsorption of AM^+; (2) increasing AM^+ concentration; and (3) varying the AM^+ identity from Li^+ to Na^+ and then to K^+ given that Li^+ weakens the Pt−O bond the least while K^+ weakens it the most.[13] The AM^+-induced destabilization of OH_{ad} coincides with the HSAB theory wherein the AM^+ promotes the OH_{ad} desorption into the bulk. Since the H_{ad} and OH_{ad} compete for active sites on monometallic Pt surfaces, the weakening Pt−OH_{ad} bond hinders the OH^- adsorption and delays the removal of H_{ad}, thus is detrimental to the HOR. Accordingly, we attribute the slower HOR kinetics of Pt/C with increasing Li^+ concentration to the Li^+-induced destabilization of OH_{ad} as per the bifunctional mechanism. The slower HOR kinetics in NaOH/KOH compared to that in LiOH (Figure 4A) can also be related to the weaker Pt−OH_{ad} bond. As for bimetallic Pt surfaces wherein the second metal is highly oxophilic such as Ni, Ru, and Ir,[23] the competition between H_{ad} and OH_{ad} for active sites is minimal since Pt hosts H_{ad} and the oxophilic metal hosts OH_{ad}. Thus, the AM^+-induced weakening of the OH_{ad} bond does not hamper the HOR significantly (Figure 3A). The beneficial role of Ni on the HOR is related to its redox transition from Ni^0 to Ni^{2+} during the HOR that promotes OH^- adsorption from the electrolyte forming OH_{ad}. Likewise, the redox transition from Ni^{2+} to Ni^0 further favors the OH_{ad} removal that is also promoted by AM^+ and thus may further benefit the HER. Collectively speaking, the redox transition of Ni within the HER/HOR kinetic potential range observed by *in situ* XAS (Figure 2) promotes the exchange of OH_{ad} with the alkaline electrolyte, thereby benefiting the HER/HOR kinetics.

If the OH_{ad}-mediated bifunctional mechanism applies to the HOR, it will also apply to the CO oxidation that is governed by the same principle: OH_{ad} facilitating oxidative removal of reducing species (H_{ad} or CO_{ad}).[8] Indeed, the CO oxidation peak of the Pt surfaces is negatively shifted to lower potentials by (1) switching the electrolyte from 0.1 M NaOH to 0.1 M LiOH;[32] (2) decreasing Li^+ concentration (Figure S11); and (3) inducing surface Ni oxides (Figure S12).[8] And all these behaviors also promote the HOR of stepped Pt surfaces.

CONCLUSIONS

In summary, the presence of OH_{ad}-$(H_2O)_x$-AM^+ adducts promotes the HER as per the HSAB theory but impedes the HOR by destabilizing the OH_{ad} as per the bifunctional mechanism. Although this so-called 2B theory is manifested here by varying the concentration and identity of AM^+, the OH_{ad}-$(H_2O)_x$-AM^+ adducts are always present for surfaces with abundant OH_{ad} in high-pH media, dictating the kinetics of the HER/HOR and many other electrochemical reactions. It is expected that the abundance and binding energy of OH_{ad} are highly sensitive to the surface structure, which may account for the high sensitivity of the alkaline HER/HOR rates of some transition metals to their surface structures. Since the abundances of OH_{ad}, OH^-, and AM^+ are pH-dependent, the 2B theory also contributes to the pH-dependent HER/HOR kinetics, together with the pzfc theory. In a large scale the HBE theory is valid, predicting the volcano trend of the HER/HOR rates in base over a broad range of elements as a function of $E_{M\text{-}H}$, like in acid. The profound cation effects on the alkaline HER/HOR kinetics of transition metal electrocatalysts demonstrated here implicate that the HER/HOR performance measured in a RDE and in an alkaline fuel cell may only be loosely related considering the dramatic difference in the cation environment between these two devices.

EXPERIMENTAL METHODS

Chemicals. Carbon-supported platinum nanoparticles (Pt/C, 47.2 wt %) were purchased from Tanaka Kikinzoku Kogyo. Carbon-supported Pt_1Ni_1 nanoparticles (Pt_1Ni_1/C, 30 wt %) were purchased from E-Tek De Nora. Nickel(II) perchlorate ($Ni(ClO_4)_2$, 98%), lithium perchlorate ($LiClO_4$, 99.99%), lithium hydroxide (LiOH, >98%), sodium hydroxide (NaOH, >98%), potassium hydroxide (KOH, 99.99%), and perchloric acid ($HClO_4$, 70%, PPT grade) were all purchased from Sigma-Aldrich. All aqueous solutions were prepared using deionized (DI) water (18.2 MΩ·cm) obtained from an ultrapure purification system (Aqua Solutions).

Preparation of Ni/C Nanoparticles. Ni metal (25%) on a carbon black support (Ketjen Black-EC600JD, Akzo Nobel Polymer Chemicals) was synthesized using a strong reducing agent (sodium borohydride, Sigma-Aldrich). First, 900 mg of carbon black was dispersed in 60 mL of H_2O (18.2 MΩ Millipore), using a 500 mL three-neck round-bottom flask (RBF), and stirred overnight for better dispersion. A 1.56 g amount of Ni chloride salt ($NiCl_2·6H_2O$, Sigma-Aldrich) was dissolved until completion in 10 mL of Mili-Q water. The solution was added to the carbon black dispersion. The RBF containing carbon black and metal salt was placed in an ice bath for at least 1 h while it was stirred continually. Nitrogen gas was bubbled into the mixture solution to prepare for an inert ambiance before the reduction process. Three moles of $NaBH_4$ (3:1 mol ratio with respect to Ni metal) was dissolved in 10 mL of H_2O dropwise to the mixture solution in the ice bath. After the solution was cooled to room temperature, it was left to stir overnight and then vacuum filtered. About 200 mL of Milli Q water was used to wash during the filtration step. The product was dried in a vacuum oven for 12 h prior to a heat treatment at 700 °C for 3 h, under Ar gas, with a ramping rate of 10 °C/min.

Electrode Preparation. The preparation of the thin-film electrodes of Pt/C, Pt_1Ni_1/C, and Ni/C followed our previous study.[11] The average particle size of the Pt/C, Pt_1Ni_1/C, and Ni/C determined by transmission electron microscopy was 2.0 ± 0.4, 4.2 ± 0.6, and 6.3 ± 0.7 nm based on around 200 particle counts. A 2−3 mg amount of catalyst powders was added into the mixture of 1 mL of DI water (18.2 MΩ·cm), 1 mL of isopropyl alcohol, and 5 μL of Nafion (5%). The aqueous suspensions were sonicated for 45 min with an ice bath, deposited onto the electrode surface with a rotation rate of 500−700 rpm, and dried in air at room temperature for 20 min to achieve a Pt or Ni loading of ∼10 μg·cm^{-2}. Prior to the electrodeposition, the glass carbon electrode embedded in PTFE or the Pt polycrystalline electrode was polished mechanically by 0.5, 0.3, and 0.05 μm alumina powder and then sonicated in sequence for 5 mins in DI water and ethanol.

Electrochemical Measurements. All the electrochemical experiments were conducted using a three-electrode cell system. The working electrode was a glassy carbon rotating disk electrode from Pine Instruments and the glassy carbon geometry area was 0.2463 cm^2 or a Pt polycrystalline from Pine Instruments with a geometry area of 0.2124 cm^2. Pt wire and Ag/AgCl (1 M Cl^-) were used as the counter and reference electrodes, respectively. All potentials reported in this paper are referenced to the reversible hydrogen electrode (RHE), calibrated in the same electrolyte by measuring the potential of the HOR/HER currents at zero corresponding to 0 V versus RHE (V_{RHE}).

Prior to the RDE testing in alkaline solution, the Pt/C and Pt polycrystalline electrodes were cycled with a rotation rate of 1600 rpm in an Ar-saturated 0.1 M $HClO_4$ electrolyte with a scan rate of 500 mV s^{-1} between the potential range of 0.05 and 1.2 V_{RHE} for 100 cycles following the Department of Energy (DOE)'s recommended protocol.[33] The Ni/C and Pt_1Ni_1/C electrodes were mildly conditioned in an Ar-saturated 0.1 M AMOH (AM = Li, Na, K)

DOI: 10.1021/jacs.8b13228
J. Am. Chem. Soc. 2019, 141, 3232−3239

electrolyte with a scan rate of 50 mV s^{-1} for 10 cycles between the potential range of 0.05 and 1.0 V_{RHE}.

HER/HOR tests were conducted in a H_2-saturated AMOH electrolyte at room temperature with a scan rate of 10 mV s^{-1} and a potential range of −1.2 (−1.3 for Ni/C)−0 V vs Ag/AgCl with a rotation rate of 2500 rpm. The CVs were recorded in Ar-saturated AMOH between 0.05 and 1.1 V_{RHE} at a scan rate of 20 mV s^{-1} after it reached the steady state. The HOR kinetic current densities (i_k) were obtained from correcting the polarization curves by the hydrogen mass transport in the HOR branch using the Koutecky−Levich equation. All the electrochemical active surface area was determined by integrating hydrogen adsorption charge on CV curves by assuming a value of 210 $\mu C \cdot cm^{-2}$ for the adsorption of one hydrogen monolayer. Double-layer correction was applied.

Impedance Measurements. The impedance spectra were measured with frequencies from 10^5 to 0.1 Hz with an amplitude of 10 mV by Autolab. Equivalent circuits were fitted to the data with Zview software. The solution resistances measured at room temperature as a function of Li^+ concentration and applied potentials were systematically evaluated.

Electrochemical Deposition of $Ni(ClO_4)_2$. After the CV and HER/HOR measurements of the Pt/C electrode, the electrode was unmounted from the RDE and immersed in 20 μM $Ni(ClO4)_2$ for 1 min. Then the HER/HOR polarization curves and the CV were recorded in a H_2/Ar-saturated 0.1 M KOH electrolyte under identical conditions as those of Pt/C. This process was repeated with increasing concentration of $Ni(ClO4)_2$ until 200 μM.

Adding $LiClO_4$. $LiClO_4$ was dissolved into 0.1 M LiOH, resulting in a concentration of 1 M $LiClO_4$ solution. A selected amount of solution was then added into the 0.1 M LiOH electrolyte (~80 mL) to vary the Li^+ concentration in the electrolyte in a controlled manner.

Acid Treatments. The as-received Pt_1Ni_1/C alloy (denoted as AR-Pt_1Ni_1/C) was either immersed and stirred in a 0.1 M $HClO_4$ solution overnight at room temperature (denoted as AI-Pt_1Ni_1/C) following the previous literature[7] or subjected to a typical CV activation in an Ar-saturated 0.1 M $HClO_4$ solution between 0.05 and 1.2 V_{RHE} for 100 cycles with a scan rate of 100 mV·s^{-1} (denoted as CA-Pt_1Ni_1/C) following the previous literature.[21]

Oxygen Reduction Reaction. ORR tests were conducted on CA-Pt_1Ni_1/C and Pt/C in an O_2-saturated 0.1 M $HClO_4$ or KOH electrolyte at room temperature with a scan rate of 20 mV s^{-1} and rotation rate of 1600 rpm. CVs were performed at room temperature in an Ar-saturated 0.1 M $HClO_4$ or KOH solution from 0.05 V_{RHE} to 1.1 (or 1.6) V_{RHE} with a sweep rate of 20 mV·s^{-1}. The ORR performance was evaluated based on the anodic scan.

CO Stripping. Before conducting the CO stripping experiments, two potential cycles between 0.05 and 1.1 V_{RHE} in 0.1 M MeOH with a scan rate of 20 mV·s^{-1} were applied to the electrode before the adsorption of carbon monoxide by dosing the gas at a constant potential of 0.05 V_{RHE} for 15 min into the solution, and then Ar was purged into the same electrolyte for 25 min at the same potential to remove the CO from the electrolyte.

***In Situ* XAS Data Collection and Analysis.** The preparation method of the XAS electrodes was the same as used in our previous work.[34] The final Pt geometric loadings were chosen to give 0.5 transmission spectra edge heights at the Pt L_3 edge. The XAS experiments were conducted at room temperature in a previously described flow half-cell[35] in which continuously H_2-purged 0.1 M KOH or O_2-purged 0.1 M $HClO_4$ was circulated. The voltage cycling limits were −0.2 to 0.8 V_{RHE}. The XAS spectra at the Pt and Ni edges of the Pt/C immersed in $Ni(ClO4)_2$ solution were collected in the transmission and fluorescence modes, respectively, at beamline 5-BM-D at the Advanced Photon Source (APS), Argonne National Laboratory (ANL). The data at the Pt and Ni edges of the Pt_1N_i/C alloy were collected in the transmission mode at beamline ISS 8-ID of the National Synchrotron Light Source (NSLS) II, Brookhaven National Laboratory (BNL). Typical experimental procedures were utilized with details provided in our previous work.[34]

■ ASSOCIATED CONTENT

Supporting Information

The Supporting Information is available free of charge on the ACS Publications website at DOI: 10.1021/jacs.8b13228.

Sample preparation, XAS and electrochemical studies on the PtNi/C alloy, *in situ* XAS studies on Ni/C, impedance measurements as a function of Li^+ concentrations, HER/HOR measurements as a function of Na^+ concentrations, and CO stripping measurements (PDF)

■ AUTHOR INFORMATION

Corresponding Author

*q.jia@neu.edu

ORCID

Ershuai Liu: 0000-0002-6491-5504
Jingkun Li: 0000-0003-1699-3089
Zeyan Liu: 0000-0001-9237-7603
Zipeng Zhao: 0000-0003-1135-6742
Yu Huang: 0000-0003-1793-0741
Sanjeev Mukerjee: 0000-0002-2980-7655
Qingying Jia: 0000-0002-4005-8894

Notes

The authors declare no competing financial interest.

■ ACKNOWLEDGMENTS

This work was supported by the Office of Naval Research (ONR) under award number N00014-18-1-2155. The authors declare no competing financial interests. Use of beamline ISS 8-ID of the National Synchrotron Light Source (NSLS) II was supported by the NSLS-II, Brookhaven National Laboratory, under U.S. DOE Contract No. DE-SC0012704. Use of beamline 5-BM-D at the Advanced Photon Source was supported by the U.S. Department of Energy, Office of Science, Office of Basic Energy Sciences, under Contract No. W-31-109-Eng-38. Q.J. acknowledges help from Eli Stavitski and Klaus Attenkofer from ISS, NSLS-II; Qing Ma from DND-CAT, APS at ANL; and Todd E. Miller and Lynne LaRochelle Richard from Northeastern University with the XAS data collection.

■ REFERENCES

(1) Erdey-Gruz, T.; Volmer, M. The theory of hydrogen overvoltage. *Z. Phys. Chem.* **1930**, *150*, 203.

(2) Trasatti, S. Work function, electronegativity, and electrochemical behaviour of metals: III. Electrolytic hydrogen evolution in acid solutions. *J. Electroanal. Chem. Interfacial Electrochem.* **1972**, *39*, 163−184.

(3) Durst, J.; Siebel, A.; Simon, C.; Hasche, F.; Herranz, J.; Gasteiger, H. A. New insights into the electrochemical hydrogen oxidation and evolution reaction mechanism. *Energy Environ. Sci.* **2014**, *7*, 2255−2260.

(4) Schmidt, T. J.; Ross, P. N.; Markovic, N. M. Temperature dependent surface electrochemistry on Pt single crystals in alkaline electrolytes: Part 2. The hydrogen evolution/oxidation reaction. *J. Electroanal. Chem.* **2002**, *524−525*, 252−260.

(5) Wang, Y.; Wang, G.; Li, G.; Huang, B.; Pan, J.; Liu, Q.; Han, J.; Xiao, L.; Lu, J.; Zhuang, L. Pt−Ru catalyzed hydrogen oxidation in alkaline media: Oxophilic effect or electronic effect? *Energy Environ. Sci.* **2015**, *8*, 177−181.

(6) Schwämmlein, J. N.; Stühmeier, B. M.; Wagenbauer, K.; Dietz, H.; Tileli, V.; Gasteiger, H. A.; El-Sayed, H. A. Origin of superior HOR/HER activity of bimetallic Pt-Ru catalysts in alkaline media

DOI: 10.1021/jacs.8b13228
J. Am. Chem. Soc. 2019, 141, 3232−3239

identified via Ru@Pt core-shell nanoparticles. *J. Electrochem. Soc.* **2018**, *165*, H229−H239.
(7) Lu, S.; Zhuang, Z. Investigating the influences of the adsorbed species on catalytic activity for hydrogen oxidation reaction in alkaline electrolyte. *J. Am. Chem. Soc.* **2017**, *139*, 5156−5163.
(8) Subbaraman, R.; Tripkovic, D.; Chang, K.-C.; Strmcnik, D.; Paulikas, A. P.; Hirunsit, P.; Chan, M.; Greeley, J.; Stamenkovic, V.; Markovic, N. M. Trends in activity for the water electrolyser reactions on 3d M (Ni, Co, Fe, Mn) hydr(oxy)oxide catalysts. *Nat. Mater.* **2012**, *11*, 550−557.
(9) Subbaraman, R.; Tripkovic, D.; Strmcnik, D.; Chang, K.-C.; Uchimura, M.; Paulikas, A. P.; Stamenkovic, V.; Markovic, N. M. Enhancing hydrogen evolution activity in water splitting by tailoring Li^+-$Ni(OH)_2$-Pt interfaces. *Science* **2011**, *334*, 1256−1260.
(10) Elbert, K.; Hu, J.; Ma, Z.; Zhang, Y.; Chen, G.; An, W.; Liu, P.; Isaacs, H. S.; Adzic, R. R.; Wang, J. X. Elucidating hydrogen oxidation/evolution kinetics in base and acid by enhanced activities at the optimized Pt shell thickness on the Ru core. *ACS Catal.* **2015**, *5*, 6764−6772.
(11) Li, J.; Ghoshal, S.; Bates, M. K.; Miller, T. E.; Davies, V.; Stavitski, E.; Attenkofer, K.; Mukerjee, S.; Ma, Z.-F.; Jia, Q. Experimental proof of the bifunctional mechanism for the hydrogen oxidation in alkaline media. *Angew. Chem., Int. Ed.* **2017**, *56*, 15594−15598.
(12) Sheng, W.; Zhuang, Z.; Gao, M.; Zheng, J.; Chen, J. G.; Yan, Y. Correlating hydrogen oxidation and evolution activity on platinum at different pH with measured hydrogen binding energy. *Nat. Commun.* **2015**, *6* DOI: 10.1038/ncomms6848.
(13) Chen, X.; McCrum, I. T.; Schwarz, K. A.; Janik, M. J.; Koper, M. T. M. Co-adsorption of cations as the cause of the apparent pH dependence of hydrogen adsorption on a stepped platinum single-crystal electrode. *Angew. Chem., Int. Ed.* **2017**, *56*, 15025−15029.
(14) McCrum, I. T.; Janik, M. J. pH and alkali cation effects on the Pt cyclic voltammogram explained using density functional theory. *J. Phys. Chem. C* **2016**, *120*, 457−471.
(15) Ledezma-Yanez, I.; Wallace, W. D. Z.; Sebastián-Pascual, P.; Climent, V.; Feliu, J. M.; Koper, M. T. M. Interfacial water reorganization as a pH-dependent descriptor of the hydrogen evolution rate on platinum electrodes. *Nat. Energy* **2017**, *2*, 17031.
(16) Van der Niet, M. J.; Garcia-Araez, N.; Hernández, J.; Feliu, J. M.; Koper, M. T. Water dissociation on well-defined platinum surfaces: the electrochemical perspective. *Catal. Today* **2013**, *202*, 105−113.
(17) Frumkin, A. N. Hydrogen overvoltage and the structure of the double layer. *Z. Phys. Chem.* **1933**, *121*, 164A.
(18) Strmcnik, D.; Uchimura, M.; Wang, C.; Subbaraman, R.; Danilovic, N.; van der, V.; Paulikas, A. P.; Stamenkovic, V. R.; Markovic, N. M. Improving the hydrogen oxidation reaction rate by promotion of hydroxyl adsorption. *Nat. Chem.* **2013**, *5*, 300−306.
(19) Zeng, Z.; Chang, K.-C.; Kubal, J.; Markovic, N. M.; Greeley, J. Stabilization of ultrathin (hydroxy) oxide films on transition metal substrates for electrochemical energy conversion. *Nat. Energy* **2017**, *2*, 17070.
(20) Cong, Y.; Yi, B.; Song, Y. Hydrogen oxidation reaction in alkaline media: from mechanism to recent electrocatalysts. *Nano Energy* **2018**, *44*, 288−303.
(21) Li, M.; Zhao, Z.; Cheng, T.; Fortunelli, A.; Chen, C.-Y.; Yu, R.; Zhang, Q.; Gu, L.; Merinov, B. V.; Lin, Z. Ultrafine jagged platinum nanowires enable ultrahigh mass activity for the oxygen reduction reaction. *Science* **2016**, *354*, 1414−1419.
(22) Danilovic, N.; Subbaraman, R.; Strmcnik, D.; Chang, K.-C.; Paulikas, A. P.; Stamenkovic, V. R.; Markovic, N. M. Enhancing the alkaline hydrogen evolution reaction activity through the bifunctionality of $Ni(OH)_2$/metal catalysts. *Angew. Chem., Int. Ed.* **2012**, *51*, 12495−12498.
(23) Danilovic, N.; Subbaraman, R.; Strmcnik, D.; Paulikas, A. P.; Myers, D.; Stamenkovic, V. R.; Markovic, N. M. The Effect of noncovalent interactions on the HOR, ORR, and HER on Ru, Ir, and $Ru_{0.50}Ir_{0.50}$ metal surfaces in alkaline environments. *Electrocatalysis* **2012**, *3*, 221−229.
(24) Strmcnik, D.; Kodama, K.; Van der Vliet, D.; Greeley, J.; Stamenkovic, V. R.; Marković, N. M. The role of non-covalent interactions in electrocatalytic fuel-cell reactions on platinum. *Nat. Chem.* **2009**, *1*, 466.
(25) Strmcnik, D.; Escudero-Escribano, M.; Kodama, K.; Stamenkovic, V. R.; Cuesta, A.; Marković, N. M. Enhanced electrocatalysis of the oxygen reduction reaction based on patterning of platinum surfaces with cyanide. *Nat. Chem.* **2010**, *2*, 880.
(26) Nørskov, J. K.; Rossmeisl, J.; Logadottir, A.; Lindqvist, L.; Kitchin, J. R.; Bligaard, T.; Jónsson, H. Origin of the overpotential for oxygen reduction at a fuel-cell cathode. *J. Phys. Chem. B* **2004**, *108*, 17886−17892.
(27) Pearson, R. G. Hard and soft acids and bases. *J. Am. Chem. Soc.* **1963**, *85*, 3533−3539.
(28) Zhao, Z.; Liu, H.; Gao, W.; Xue, W.; Liu, Z.; Huang, J.; Pan, X.; Huang, Y. Surface-engineered PtNi-O nanostructure with record-High performance for electrocatalytic hydrogen evolution reaction. *J. Am. Chem. Soc.* **2018**, *140*, 9046−9050.
(29) Liang, Z.; Ahn, H. S.; Bard, A. J. A Study of the mechanism of the hydrogen evolution reaction on nickel by surface interrogation scanning electrochemical microscopy. *J. Am. Chem. Soc.* **2017**, *139*, 4854−4858.
(30) Intikhab, S.; Snyder, J. D.; Tang, M. H. Adsorbed hydroxide does not participate in the volmer step of alkaline hydrogen electrocatalysis. *ACS Catal.* **2017**, *7*, 8314−8319.
(31) Rebollar, L.; Intikhab, S.; Snyder, J. D.; Tang, M. H. Determining the viability of hydroxide-mediated bifunctional HER/HOR mechanisms through single-crystal voltammetry and micro-kinetic modeling. *J. Electrochem. Soc.* **2018**, *165*, J3209−J3221.
(32) Stoffelsma, C.; Rodriguez, P.; Garcia, G.; Garcia-Araez, N.; Strmcnik, D.; Marković, N. M.; Koper, M. T. M. Promotion of the oxidation of carbon monoxide at stepped platinum single-crystal electrodes in alkaline media by lithium and beryllium cations. *J. Am. Chem. Soc.* **2010**, *132*, 16127−16133.
(33) Kocha, S. S.; Shinozaki, K.; Zack, J. W.; Myers, D. J.; Kariuki, N. N.; Nowicki, T.; Stamenkovic, V.; Kang, Y.; Li, D.; Papageorgopoulos, D. Best practices and testing protocols for benchmarking ORR activities of fuel cell electrocatalysts using rotating disk electrode. *Electrocatalysis* **2017**, *8*, 366−374.
(34) Jia, Q.; Liang, W.; Bates, M. K.; Mani, P.; Lee, W.; Mukerjee, S. Activity descriptor identification for oxygen reduction on platinum-based bimetallic Nanoparticles: in situ observation of the linear composition−strain−activity relationship. *ACS Nano* **2015**, *9*, 387−400.
(35) Arruda, T. M.; Shyam, B.; Lawton, J. S.; Ramaswamy, N.; Budil, D. E.; Ramaker, D. E.; Mukerjee, S. Fundamental aspects of spontaneous cathodic deposition of Ru onto Pt/C electrocatalysts and membranes under direct methanol fuel cell operating conditions: an in situ x-ray absorption spectroscopy and electron spin resonance study. *J. Phys. Chem. C* **2010**, *114*, 1028−1040.

DOI: 10.1021/jacs.8b13228
J. Am. Chem. Soc. 2019, 141, 3232−3239